European **J**ournal of **Chem**istry

Describing auxin solid-state intermolecular interactions using contact descriptors, shape properties, molecular fingerprint, and interaction energy: Comparison of pure auxin crystal and auxin-TIR1 co-crystal

Kodjo Djidjolé Etsè [1], Koffi Sénam Etsè [2,*] and Marie-Luce Akossiwoa Quashie [1]

[1] *Faculty of Sciences, Laboratory of Forest Research, Unit Physiology-Horticulture-Biotechnology, University of Lome, Lome, 1515, Togo*
[2] *Department of Pharmacy, Faculty of Medicine, Laboratory of Medicinal Chemistry, CIRM, University of Liège, Liège, 4000, Belgium*

* Corresponding author at: Department of Pharmacy, Faculty of Medicine, Laboratory of Medicinal Chemistry, CIRM, University of Liège, Liège, 4000, Belgium.
 e-mail: ks.etse@uliege.be (K.S. Etsè).

RESEARCH ARTICLE

ABSTRACT

This work reports for the first time, the analysis of intermolecular interactions in crystal structures of auxin (Indole-3-acetic acid) crystallized as pure sample (Aux-A) or co-crystallized with transport inhibitor response 1 (Aux-B). Using crystal packing of pure auxin and a cluster of residues in a radius of 6 Å around this ligand in the transport inhibitor response 1 binding domain, various properties were calculated and mapped on the Hirshfeld surface (HS). The HSs of the two molecules are characterized by close parameters of volume, area, globularity, and asphericity revealing the efficiency of the considered cluster. The HS mapped over descriptors like d_e, d_i and d_{norm} showed red spots corresponding to hydrogen bonds contacts. In addition to the shape index and curvedness descriptors, the results highlight weak interactions stabilizing the auxin structures. The analyses of electrostatic potential, electron density, and deformation density maps confirm the slightly change in the electron donor and acceptor groups localization. Furthermore, the molecular fingerprint analyses revealed a notable discrepancy in the shape and percentage value of the various contacts. Decomposition of the fingerprint shows that the contributions of important contacts (H···H, H···O, and O···O) are higher in Aux-B than in Aux-A. Finally, the quantitative approach by the determination of the molecular interaction energies of the two structures in their respective crystallographic environment revealed that Aux-A is slightly more stabilized than Aux-B.

1. Introduction

The vitro plants' production has emerged as an alternative way to counterbalance the low germination and multiplication observed in some vegetables [1]. It was shown that phytohormones are important molecules implicated in different physiological mechanisms in plants [2]. Phytohormones are therefore highly essential since they play an important role in plants' growth, development, stress, and defense responses [3]. Phytohormones are represented by various families of chemical compounds like auxin, abscisic acid, cytokinin, gibberellin, ethylene, brassinosteroid, jasmonate, and strigolactone [4-6]. Auxin derivatives received special attention thanks to their importance in plant grow and development [7-9]. In addition to the natural auxin (Indole-3-acetic acid), a variety of synthetic derivatives based on the indole backbone are described showing the ability to bind to the transport inhibitor response 1 (TIR1) receptor [10,11].

Auxin is recognized to interact with various transporters implicated in plants' physiological processes [12,13]. Therefore, the perception, the mechanism, and the role of auxin in plants growth and development were explored [14,15]. In this line, Tan and coworkers reported the crystal structure of the *Arabidopsis* TIR1-ASK1 complexed with auxin [16]. The interactions of auxin with the residues of TIR1 binding domain is explored thanks to crystallographic parameters and the proximity of functional groups [16]. To get more insight about the structural features of that phytohormone, its molecular structure was determined thanks to X-ray diffraction analysis [17,18]. Recently, Nigovic and coworkers have resolved and deposited a novel structure of auxin and performed its DFT calculation [19]. Although the chemical structure of auxin is described, studies describing the intermolecular interactions using contacts, shape, and surface property descriptors are not reported at all. In addition, the crystal structure of this ligand enclosed in various receptors is reported without using these descriptors [16,20]. Indeed, describing contact interactions using the Hirshfeld surface has emerged as a powerful way to depict close contacts like hydrogen bonds, π-π stabilization, acceptor, and donor group localization [21]. In addition, for a selected molecule, the contribution of all contacts atom pairs-wise can be combined to form two-dimensional molecular fingerprints that are highly sensitive to the chemical environment [22].

Figure 1. Molecular structure of the auxin (a) and the cartoon representation of the cluster surrounding the auxin (in magenta) in TIR1 receptor (b).

Analyzing the results provided by these techniques could give more information about the interaction features that could be helped to correlate contacts, stability, and activity.

The present work aims therefore to describe the interactions observed in the auxin crystal structure and to expose its molecular fingerprint. To get more insight about the interactions of auxin with transport inhibitor response 1 (TIR1), this work will also describe and compare the intermolecular interactions thanks to contact regions, the surface shape, and molecular fingerprint of isolated and co-crystallized auxin in TIR1. These interactions will be correlated to the electron density modification. Finally, the quantification of intermolecular energies will be used to complete the characterization of the two structures.

2. Experimental

The Hirshfeld surfaces (HSs) mapped over different properties like d_i, d_e, d_{norm}, shape-index, electron, and deformation density, and the 2D fingerprint plots were generated using CrystalExplorer 17.5 [23] and the data were obtained according to the procedure previously described [24]. The co-crystal structure of auxin with TIR1 (PDB code 2P1Q, resolution of 1.91 Å) retrieved from the protein data bank (PDB) was used in the study [16]. The PyMOL software was used for the molecular cluster preparation [25]. Briefly, a cluster formed by the residues surrounding the auxin ligand was selected and saved in pdb format. Hydrogen atoms were added to the molecules as well as to oxygen atoms of water molecules using the "Add Hydrogen" utility tool in PyMOL. The presence of water molecules is maintained to generate different shape and contact surfaces. The final pdb file is then converted in a cif file to allow analyses with the CrystalExplorer program. The cif file containing the crystal structure of pure auxin was retrieved from CCDC with the ID:141657 [19]. Electron density, deformation density, and electrostatic potentials map are calculated at the B3LYP/6-31G(d,p) level of theory. The interaction energy calculation was achieved using the CrystalExplorer software within 3.8 Å molecular cluster centering on the selected auxin molecule.

3. Results and discussion

The interaction between auxin and TIR1 receptor was explored thanks to the co-crystal studies reported by Tan and coworkers [16], where the analyses were achieved by considering crystallographic parameters and short distances to highlight interacting residues. Overall consideration made, the hydrogen bonds, noncovalent, Van der Walls contacts and π-π stacking are conditioned by a distance shorter than 4 Å [26,27]. Hence, in this study, we considered a cluster formed by residues and water molecules around the auxin with a radius of 6 Å. In that condition, all three space directions are occupied. That condition is mandatory to generate a well-defined and concise

HS [28,29]. The molecular structure of the auxin and the cartoon representation of the cluster surrounding the auxin in TIR1 are shown in Figure 1.

Contact descriptors are used in crystallography, DFT, and drug discovery analyses to identify the more important contacts, interactions, and noncovalent interactions that are at the origin of structure stabilization [28]. In this line, short contact descriptors like d_i, d_e, and d_{norm} are combined to the shape descriptors and surface properties such as the Shape index and the electrostatic potential mapped on the Hirshfeld surface (HS) to describe the molecular environment of various structures [21,22]. HS analysis is therefore a very good way to visualize interactions in the solid-state. Molecular HS in the crystal structure was built based on the electron distribution calculated as the sum of spherical atom electron densities [30].

The HS of auxin in TIR1 binding domain by considering the cluster was calculated and presented in Figure 2a. The HS is characterized by parameters of volume, area, globularity, and asphericity of 216.64 A³, 212.52 A², 0.821, 0.100. The HS mapped over the normalized contact descriptor d_{norm} (Figure 2b) highlight a red spot on the surface corresponding to hydrogen bonds between residues Arg403, Ser438, and Leu439 and the auxin. These interactions confirm those reported by Tan and coworkers [16]. The white and blue regions on the surface mapped over d_{norm} indicate interactions at the distance equal and longer than Van der Wall radii, respectively [31]. The electron-rich (red) and deficient (blue) domains are identified on the HS mapped over electrostatic potential as shown in Figure 2c.

For better visualization and comparison of the different surfaces, the residues will be removed from the further representtations. The distance from the surface to the nearest nucleus external to the surface (d_e), the distance to the nearest nucleus internal to the surface (d_i), as well as the normalized contact distance (d_{norm}) were calculated to reveal the regions of intermolecular interactions on the HS. The surfaces are obtained for the isolated pure crystal of auxin (Aux-A) and compared to those generated by considering the auxin in TIR1 (Aux-B). The HSs properties of Aux-A and Aux-B are characterized by close values. The values of volume, area, globularity, and asphericity are 216.64 Å³, 212.52 Å², 0.821, and 0.100, respectively, for Aux-A. These close values reveal that the cluster considered for the analyses of Aux-B is efficient to mimic the crystallographic environment of the pure form of auxin. The results show that the red spots observed around the carbonyl oxygen atoms on the surface mapped over d_i, d_e, and d_{norm}, are similar for the two compounds. On contrary, the other contacts are quite different. These observations could be predicted since, in the ligand-binding domain, auxin interactions are governed by the residues surrounding the functional groups. The lack of red spot localized in the center of the phenyl ring of the HS mapped over d_{norm} of Aux-B reveals that no X···π interaction is present.
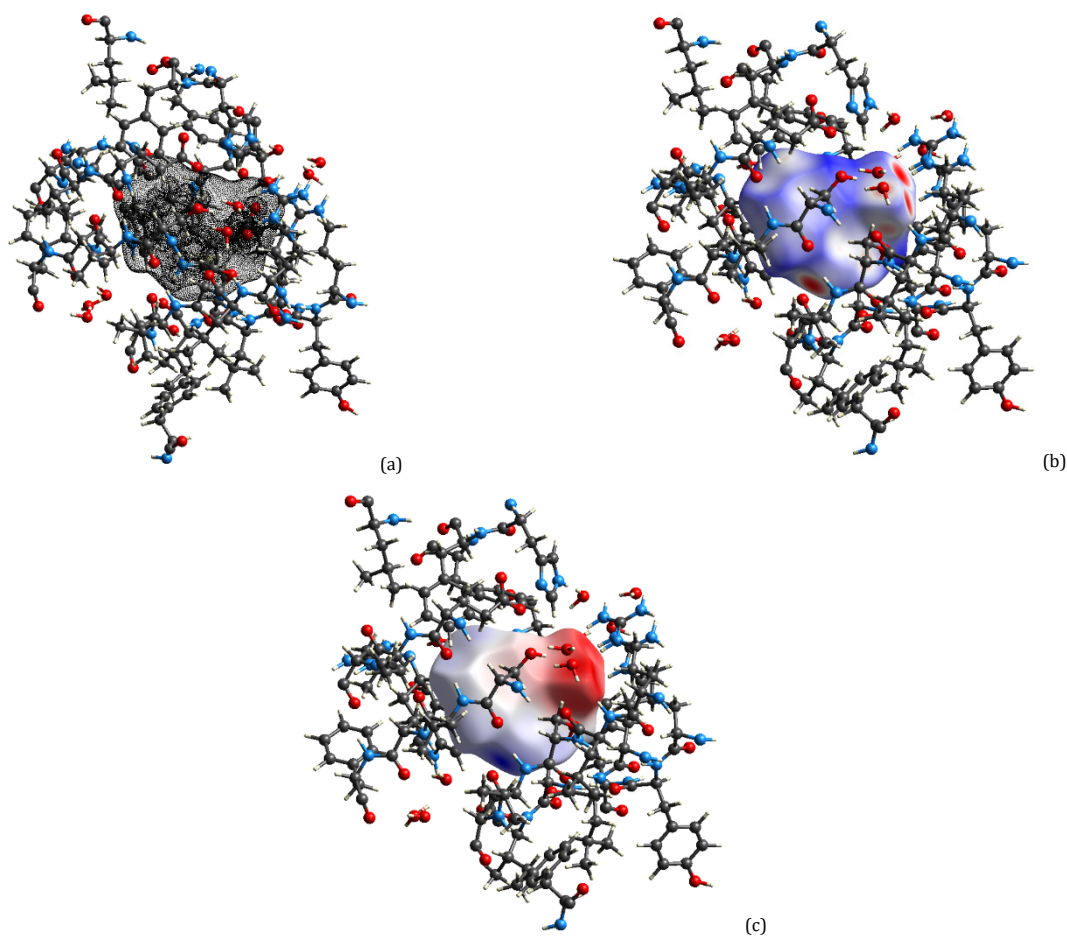
Figure 2. Hirshfeld surface (a) mapped over d_{norm} (b) and electrostatic potential (c) of the auxin generated by considering a cluster of 6 Å radius in the co-crystallized auxin-TIR1.

On contrary, the red spots observed around the N-H atom confirm the existence of a hydrogen bond with Leu439 [16].

The HS can be mapped over other properties color-coded to identify weak contacts. The property called shape index is sensitive to very subtle changes in surface shape. This property is based on the local curvature of the surface due to contacts provided by donor and acceptor atoms [32,33]. On the HS mapped with shape index of auxin, convex blue regions represent donor groups and concave red regions represent acceptor groups. The concave red regions localized in the middle of the aromatic ring of Aux-A confirm the N-H⋯π interaction with the phenyl group behaving as the acceptor group. On the HS of Aux-B, concave red domains are distributed on the surface, especially on the indole ring as well as around the two oxygen atoms of the acid group. Contrary to Aux-B, only one concave red region is observed around the carboxylic acid in Aux-A, since in Aux-B the acid group is in carboxylate form. This characteristic will be better described by considering other properties like electron density, electrostatic potential, and electron deformation density. Finally, on HS mapped over the shape index of Aux-A and Aux-B, no adjacent blue and red colored triangles are observed highlighting the absence of π-π ring stacking interaction [34]. This result contrast with that reported by Tan and coworkers which suggested that the auxin indole ring interacts with the phenyl ring of two TIR1 phenylalanine residues (Phe79 and Phe82) [16].

The existence of various residues surrounding Aux-B are at the origin of high curvature domains observed on the HS mapped over curvedness. Indeed, curvedness measures ''*how much shape*'' property could be obtained and mapped on the HS

as shown in Figure 3 [35]. Curvedness property identify on the surface, patches associated to different molecule-molecule close contacts as regions in green divided by blue boundaries. On HS mapped over curvedness of Aux-B, many curvatures domains (high values of curvedness) divide the surface into patches that could be associated with low and directional interactions with other neighbor molecules. For Aux-A, the N−H⋯π interaction is evidenced by the presence of a flat domain with a light blue point in the center of the patches localized on the phenyl ring.

Interactions and reactivity of the inhibitor are generally linked to the electronic properties, electron distribution, and electrostatic forces. To get more insight about the localization of reactive groups in auxin, these properties were calculated at the B3LYP/6-31G(d,p) level of theory and mapped on the Hirshfeld surfaces (Figure 4).

Literature data reveals that the electrostatic potential property mapped on HS could provide direct insight onto intermolecular interactions in crystals with a quantitative evaluation of the electron-rich and electron-deficient sites. The blue and red colors on the surface indicate the positive and negative potentials, respectively [36]. Contrary to Aux-B where the negative potential in mainly localized on the carboxylate oxygen group, in Aux-A, the negative potential is localized on the C=O oxygen atom and partially diffused on the heterocyclic. Moreover, electron deficiency is observed on N-H and O-H hydrogen atoms in Aux-B and Aux-A respectively (Figure 4). These results suggest that the reactivity of the two forms could not be efficiently predicted base on the calculation made using only data from Aux-A.
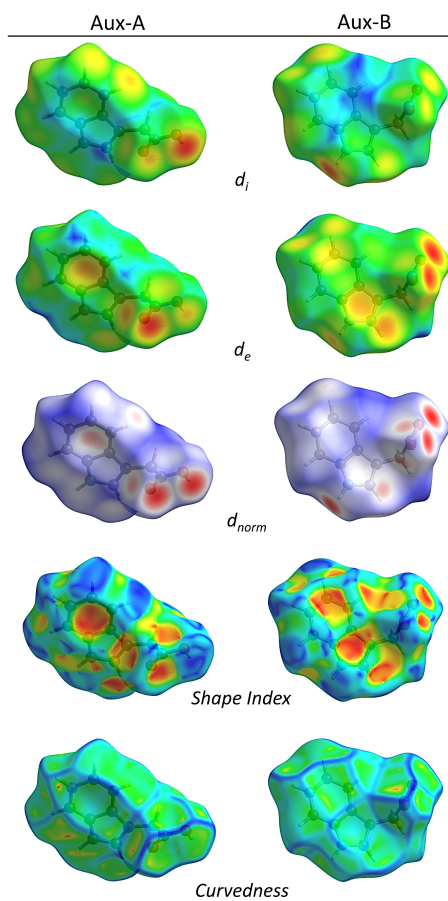
Figure 3. The Hirshfeld surface of auxin mapped over d_i in the range 0.6523 to 2.5427 Å, d_e in the range 0.6510 to 2.4436 Å, d_{norm} in the range −0.7370 to 1.2144, Shape index (−1 to +1) and curvedness (−4 to +4).
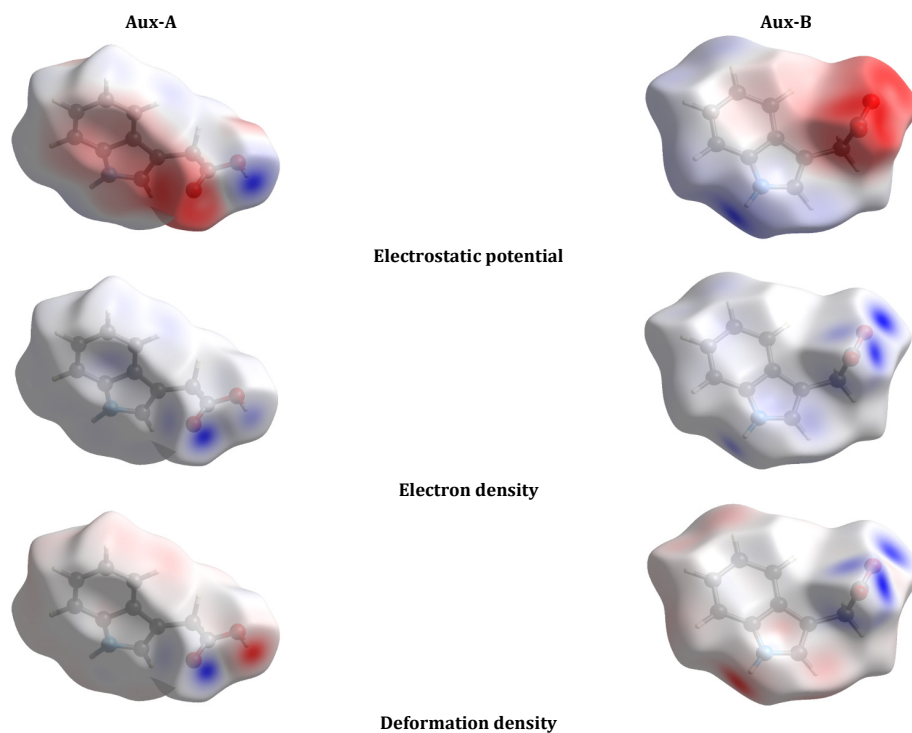
Figure 4. Hirshfeld surface mapped over electrostatic potential, electron density and deformation density of Aux-A (left) and Aux-B (right) in the range of -0.0866 to 0.2480 au.
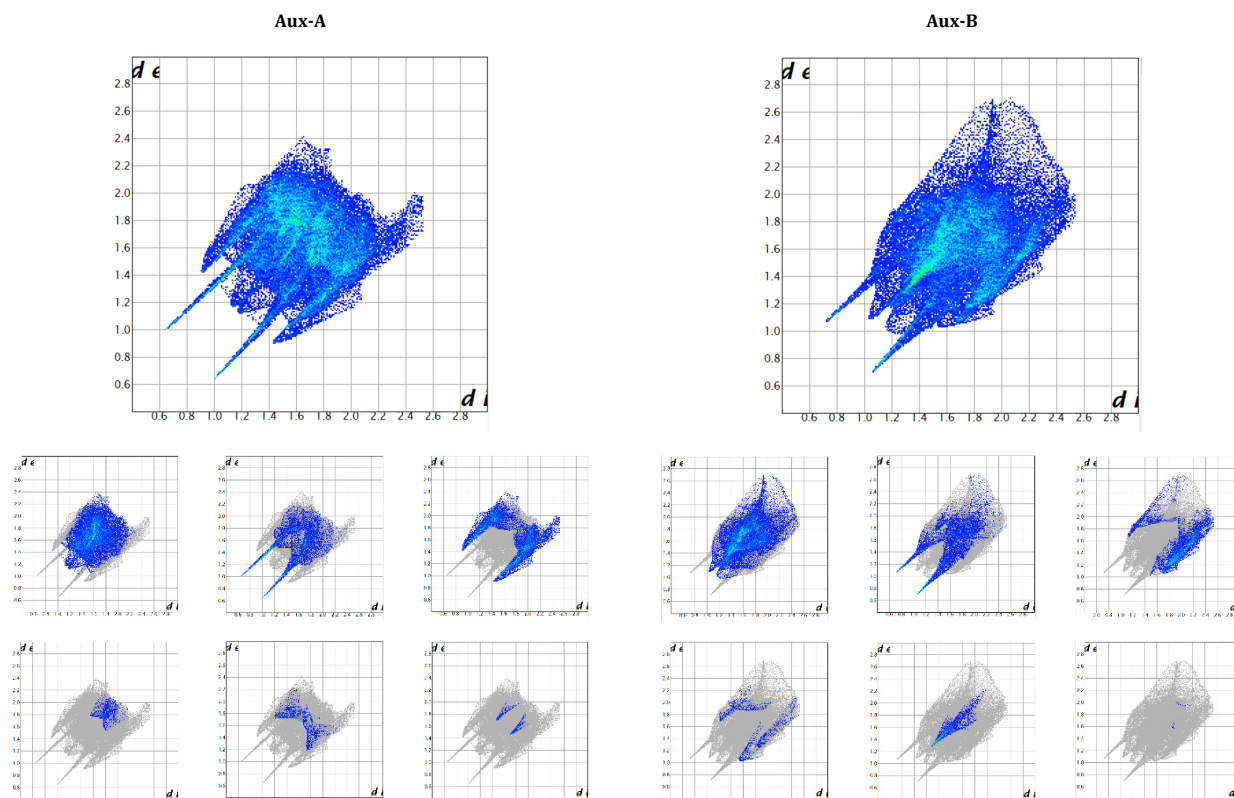
Aux-A   **Aux-B**

Figure 5. Full and decomposed 2-dimentional molecular fingerprint plots of Aux-A and Aux-B.

In addition, the existence of more blue spots in the HS mapped over the electron density showed that in Aux-B one can predict on these regions short contacts derived by electrostatic forces.

The effect of molecular environment leads to the perturbation of the electrostatic potential that can be described thanks to the deformation density surface analysis. Indeed, the deformation density that is defined as the difference between the total electron density of a molecule and the electron density of *neutral spherical unperturbed atoms* superimposed at the same atomic positions of the molecule [37] is calculated at B3LYP/6-31G(d,p) level of theory and mapped on the HS. The surface displays blue (positive) regions corresponding to local increase of electron density whereas red (negative) spots allow to depict the decrease of this density. On the COO*H* hydrogen atom of Aux-A and N*H* hydrogen atom of Aux-B, it appears an increasing of the electron density since these hydrogen atoms are implicated in hydrogen bonding. In contrary, all oxygen atoms of the carboxylate group in Aux-B are subject to electron density decrease.

Whether organic compound crystallized as pure sample or crystallized in receptor binding domain, the intermolecular contacts induce deformation of electron density, structural conformation modification and stabilization. For a best description and measure the weight of the different contacts, the molecular fingerprint is generally used. Indeed, the d_e and d_i are combined to generate a 2D histogram named molecular fingerprint (FP) plot [38,39]. Due the molecular diversity in the immediate environment, the fingerprint of a selected molecule is unique. Therefore, the full and decomposed fingerprint plot is used to understand short interactions and allow better comparison.

The molecular FP of Aux-A and Aux-B are reported on Figure 5. Analysis of these results showed notable discrepancies. In addition to the general shape, the domain of the fingerprint in the region of d_e and d_i higher that 1.4 Å is clearly different. To get more insight about these discrepancies, the

decomposed fingerprints are obtained and analyzed. The results show that full and decomposed fingerprints shape and contribution percentage are different. The shape of H···H contact histogram shows grouped pixels in the region of d_e and d_i from 1.2 to 2.2 Å with a contribution percentage of 40.8% for Aux-A in contrary to a more spread out histogram for the same contact in Aux-B. For Aux-B, the H···H contact shows higher percentage (49.5%) probably due to the diversity of hydrophobic contacts with hydrogen atoms of the residues forming the TIR1 ligand binding domain. The H···O contacts FP component results confirm the discrepancy observed although the plot shape in the region of d_e and d_i between 1 to 1.6 Å seems to be the same for the two molecules. The slightly higher percentage of H···O contacts in Aux-B (21.1%) can be attributed to hydrogen bonds in addition to those provided by the two oxygen atoms of the carboxylate group and water molecules. The increasing of the percentage of H···H and H···O contacts in Aux-B reduces that of H···C interactions, giving 30% and 20.2% for Aux-A and Aux-B respectively. The contribution of O···O contacts obtained for Aux-B is almost the double of that observed in Aux-A highlighting the additional contribution of co-crystallized water molecules (Figure 2b). Other important contacts are shown in Figure 5. Altogether, these results suggested that the molecular FP of the isolated drug could be notably different from that obtained for the drug co-crystallized with a receptor. These observations could be attributed to conformational change, diversity of neighboring and the presence of water molecules.

Although the values of the decomposed molecular fingerprint components give a pseudoquantitative weight of the various types of contacts, the calculation of the interaction energy profile of the two structures could help to get better understand about the stabilization features [40-42]. Therefore, the intermolecular interaction energies for Aux-A and Aux-B are calculated using HF/3-21G level of theory energy model available in Crystal-Explorer (CE) functionality [23].

Table 1. Color coded interacting molecules with Aux-A [Interaction energies components (*E*), rotational symmetry operations with respect to the reference molecule (S_{ymop}), the centroid-to-centroid distance between the reference molecule and interacting molecules (R) as well as the number of pair(s) of interacting molecules with respect to the reference molecule (N)].
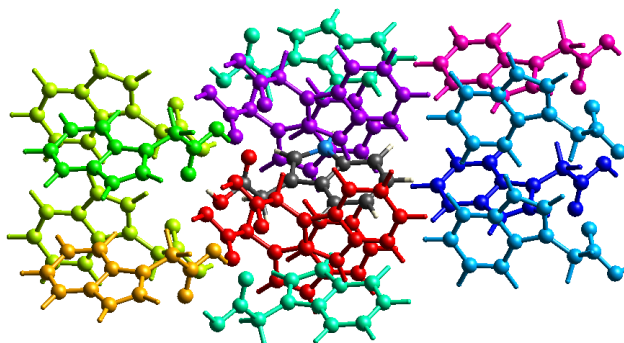
Color	N	Symop	R	E_{ele}	E_{pol}	E_{dis}	E_{rep}	E_{tot}
	2	*x, -y+1/2, z+1/2*	5.31	-3.2	-2.9	-27.7	18.2	-15.4
	1	*-x, -y, -z*	9.93	-3.0	-0.3	-2.9	0.2	-5.7
	2	*-x, y+1/2, -z+1/2*	8.36	-2.0	-1.6	-11.5	3.6	-10.6
	1	*-x, -y, -z*	8.62	-128.4	-40.2	-12.6	116.0	-74.3
	2	*x, y, z*	5.18	-7.2	-5.2	-25.2	10.5	-25.0
	2	*-x, y+1/2, -z+1/2*	10.08	-1.9	-0.3	-8.4	4.2	-6.3
	1	*-x, -y, -z*	9.34	-3.0	-0.7	-8.4	2.6	-9.0
	2	*x, -y+1/2, z+1/2*	5.55	-33.4	-10.6	-24.8	27.8	-40.7
	1	*-x, -y, -z*	10.80	1.3	-0.2	-1.7	0.1	-0.4
Total				-180.8	-62.0	-123.2	183.2	-187.4

Table 2. Color-coded interacting molecules with Aux-B [Interaction energy components (*E*), the centroid-to-centroid distance between the reference molecule and interacting molecules (R), as well as the number of pair(s) of interacting molecules with respect to the reference molecule (N)].
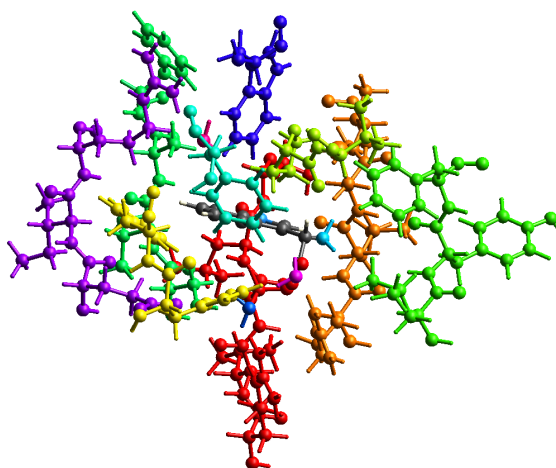
Color	N	R	E_{ele}	E_{pol}	E_{dis}	E_{rep}	E_{tot}
	1	5.83	-121.0	-62.3	-42.5	53.9	-158.4
	1	7.95	-13.6	-4.1	-14.1	9.6	-21.5
	1	9.13	-9.7	-4.8	-10.4	2.0	-20.8
	1	5.42	38.3	-6.6	-3.4	10.5	40.2
	1	7.79	2.0	-1.1	-13.0	4.5	-6.7
	1	6.56	-2.6	-0.2	-0.9	0.0	-3.7
Total			-106.6	-79.1	-84.3	80.5	-170.9

The total intermolecular energy E_{tot} (kJ/mol) relative to the reference auxin molecule (in black in Tables 1 and 2) is the sum of energies of four main components, comprising electrostatic (E_{ele}), polarization (E_{pol}), dispersion (E_{dis}) and exchange-repulsion (E_{rep}) [43] with scale factors of 1.019, 0.651, 0.901 and 0.811, respectively [44]. As shown in Tables 1 and 2, upon completion of the energy calculations, the interacting molecules are color-coded to uniquely identify them with the energy and energy components.

The results gave total interaction energy of -187.4 and -170.9 kJ/mol for Aux-A and Aux-B, respectively. It appears that the Aux-A is more stabilized in the pure crystal form than in the binding domain of TIR1. In the crystal structure of Aux-A, the packing around the selected molecule is based on the symmetrical arrangement in the three-dimensional direction. The stacking derived therefore from a very well organization of the molecules leading to high stabilization. In addition, Hirshfeld surface analyses reveal N−H···π stabilizing interactions in Aux-A crystal structure that are in contrary absent in Aux-B/TIR1 contacts. On the other hand, the environment of Aux-B is mainly defined by the binding domain volume, shape, and functional groups orientation. The geometrical constraints of the residue loop in TIR1 could reduce the stabilization of Aux-B. Nevertheless, these energies values reveal that the interactions of Aux-B with TRI1 residues are much strong to stabilize the structure with the energy tending to that of the pure form. Whether considered a form of auxin, it appears that the main contribution in the total energy (Tables 1 and 2) comes from E_{ele} (-180.8 and -106.6 kJ/mol for Aux-A and Aux-B, respectively).

4. Conclusion

A novel approach to study and described intermolecular interactions in the crystal structure of pure auxin and in the auxin-TIR1 co-crystal is present in this work. A cluster consisting by residues around the auxin in the radius of 6 Å obtained from the auxin-TIR1co-crystal allowed very good consideration of all potential interactions. The interactions are analyzed using contact descriptors, shape, and electronic properties. Results revealed that interactions in the solid-state crystal environment are different when comparing the pure or co-crystallized auxin structure. Interestingly, although the contact descriptors of d_e, d_i, d_{norm}, shape index, and curvedness revealed various contacts and confirmed previous studies, the results we present does not show the existence of any π-π stacking in the auxin co-crystallized in TIR1. The HS mapped over the electrostatic potential surface highlights that the carboxylate form of auxin provides a localized electron-rich domain observed around the oxygen atoms. Using molecular fingerprint, the present study suggested that when co-crystallized in the receptor, the H···H, H···O, and O···O interactions contribution in the overall contacts increase due to the diversity, the variety of residues and water molecules. Quantitative interaction energy calculations showed that the Aux-A is slightly more stabilized than Aux-B. The interaction of Aux-B with TIR1 is therefore sufficient to stabilize this ligand, justifying its ability to bind to the transport inhibitor response 1. Finally, this work exposes a novel way to understand and enhance the comprehension of interactions in the crystal state of auxin. Thanks to this information, a comparison between other auxin derivatives in receptors should be further performed in view to correlate the interaction energy and to identify specific contacts that could enhance the activity of these phytohormones.

Disclosure statement DS

Conflict of interest: The authors declare that they have no conflict of interest.

CRediT authorship contribution statement CR

Conceptualization: Etsè Koffi Sénam, Etsè Kodjo Djidjolé; Methodology: Etsè Koffi Sénam, Etsè Kodjo Djidjolé; Software: Etsè Koffi Sénam; Validation: Etsè Koffi Sénam, Etsè Kodjo Djidjolé; Formal Analysis: Etsè Koffi Sénam, Etsè Kodjo Djidjolé, Quashie Marie-Luce Akossiwoa; Investigation: Etsè Koffi Sénam, Etsè Kodjo Djidjolé; Resources: Etsè Koffi Sénam, Etsè Kodjo Djidjolé, Quashie Marie-Luce Akossiwoa; Data Curation: Etsè Koffi Sénam, Etsè Kodjo Djidjolé, Quashie Marie-Luce Akossiwoa; Writing - Original Draft: Etsè Koffi Sénam, Etsè Kodjo Djidjolé; Writing - Review and Editing: Etsè Koffi Sénam, Etsè Kodjo Djidjolé; Visualization: Etsè Koffi Sénam, Etsè Kodjo Djidjolé, Quashie Marie-Luce Akossiwoa; Funding acquisition: Etsè Kodjo Djidjolé; Supervision: Etsè Koffi Sénam, Quashie Marie-Luce; Project Administration: Etsè Koffi Sénam.

ORCID iD and Email ✉

Kodjo Djidjolé Etsè
✉ kodjo.etse@yahoo.fr
iD https://orcid.org/0000-0003-2145-8523
Koffi Sénam Etsè
✉ ks.etse@yahoo.com
✉ ks.etse@uliege.be
iD https://orcid.org/0000-0001-8495-4327
Marie-Luce Akossiwoa Quashie
✉ marielucequashie@gmail.com
iD https://orcid.org/0000-0003-3782-6255

References

[1].   Altpeter, F.; Springer, N. M.; Bartley, L. E.; Blechl, A.; Brutnell, T. P.; Citovsky, V.; Conrad, L.; Gelvin, S. B.; Jackson, D.; Kausch, A. P.; Lemaux, P. G.; Medford, J. I.; Orozo-Cardenas, M.; Tricoli, D.; VanEck, J.; Voytas, D. F.; Walbot, V.; Wang, K.; Zhang, Z. J.; Stewart, C. N., Jr Advancing crop transformation in the era of genome editing. *Plant Cell* **2016**, *28*, 1510–1520.

[2].   Wani, S. H.; Kumar, V.; Shriram, V.; Sah, S. K. Phytohormones and their metabolic engineering for abiotic stress tolerance in crop plants. *Crop J.* **2016**, *4*, 162–176.

[3].   Vert, G.; Nemhauser, J. L.; Geldner, N.; Hong, F.; Chory, J. Molecular mechanisms of steroid hormone signaling in plants. *Annu. Rev. Cell Dev. Biol.* **2005**, *21*, 177–201.

[4].   Browse, J. Jasmonate: An oxylipin signal with many roles in plants. In *Plant Hormones*; Elsevier, 2005; pp. 431–456.

[5].   Gomez-Roldan, V.; Fermas, S.; Brewer, P. B.; Puech-Pagès, V.; Dun, E. A.; Pillot, J.-P.; Letisse, F.; Matusova, R.; Danoun, S.; Portais, J.-C.; Bouwmeester, H.; Bécard, G.; Beveridge, C. A.; Rameau, C.; Rochange, S. F. Strigolactone inhibition of shoot branching. *Nature* **2008**, *455*, 189–194.

[6].   Umehara, M.; Hanada, A.; Yoshida, S.; Akiyama, K.; Arite, T.; Takeda-Kamiya, N.; Magome, H.; Kamiya, Y.; Shirasu, K.; Yoneyama, K.; Kyozuka, J.; Yamaguchi, S. Inhibition of shoot branching by new terpenoid plant hormones. *Nature* **2008**, *455*, 195–200.

[7].   Leyser, O. The power of auxin in plants: Figure 1. *Plant Physiol.* **2010**, *154*, 501–505.

[8].   Vanneste, S.; Friml, J. Auxin: a trigger for change in plant development. *Cell* **2009**, *136*, 1005–1016.

[9].   Paque, S.; Weijers, D. Q&A: Auxin: the plant molecule that influences almost anything. *BMC Biol.* **2016**, *14*, 67.

[10]. Yamada, R.; Murai, K.; Uchida, N.; Takahashi, K.; Iwasaki, R.; Tada, Y.; Kinoshita, T.; Itami, K.; Torii, K. U.; Hagihara, S. A super strong engineered auxin–TIR1 pair. *Plant Cell Physiol.* **2018**, *59*, 1538–1544.

[11]. Hayashi, K.-I.; Neve, J.; Hirose, M.; Kuboki, A.; Shimada, Y.; Kepinski, S.; Nozaki, H. Rational design of an auxin antagonist of the SCFTIR1 auxin receptor complex. *ACS Chem. Biol.* **2012**, *7*, 590–598.

[12]. Zazimalova, E.; Murphy, A. S.; Yang, H.; Hoyerova, K.; Hosek, P. Auxin transporters--why so many? *Cold Spring Harb. Perspect. Biol.* **2010**, *2*, a001552–a001552.

[13]. Zhao, Y. Auxin biosynthesis and its role in plant development. *Annu. Rev. Plant Biol.* **2010**, *61*, 49–64.

[14]. Salehin, M.; Bagchi, R.; Estelle, M. SCFTIR1/AFB-based auxin perception: Mechanism and role in plant growth and development. *Plant Cell* **2015**, *27*, 9–19.

[15]. Lavy, M.; Estelle, M. Mechanisms of auxin signaling. *Development* **2016**, *143*, 3226–3229.

[16]. Tan, X.; Calderon-Villalobos, L. I. A.; Sharon, M.; Zheng, C.; Robinson, C. V.; Estelle, M.; Zheng, N. Mechanism of auxin perception by the TIR1 ubiquitin ligase. *Nature* **2007**, *446*, 640–645.

[17]. Karle, I. L.; Britts, K.; Gum, P. Crystal and molecular structure of 3-indolylacetic acid. *Acta Crystallogr.* **1964**, *17*, 496–499.

[18]. Chandrasekhar, K.; Raghunathan, S. A reinvestigation of the structure of (3-indolyl)acetic acid. *Acta Crystallogr. B* **1982**, *38*, 2534–2535.

[19]. Nigović, B.; Antolić, S.; Kojić-Prodić, B.; Kiralj, R.; Magnus, V.; Salopek-Sondi, B. Correlation of structural and physico-chemical parameters with the bioactivity of alkylated derivatives of indole-3-acetic acid, a phytohormone (auxin). *Acta Crystallogr. B* **2000**, *56*, 94–111.

[20]. Woodward, A. W. Auxin: Regulation, action, and interaction. *Ann. Bot.* **2005**, *95*, 707–735.

[21]. McKinnon, J. J.; Spackman, M. A.; Mitchell, A. S. Novel tools for visualizing and exploring intermolecular interactions in molecular crystals. *Acta Crystallogr. B* **2004**, *60*, 627–668.

[22]. Ozochukwu, I. S.; Okpareke, O. C.; Izuogu, D. C.; Ibezim, A.; Ujam, O. T.; Asegbeloyin, J. N. N'-(Pyridin-3-ylmethylene)benzenesulfonohydrazide: Crystal structure, DFT, Hirshfeld surface and in silico anticancer studies. *Eur. J. Chem.* **2021**, *12*, 256–264.

[23]. Spackman, P. R.; Turner, M. J.; McKinnon, J. J.; Wolff, S. K.; Grimwood, D. J.; Jayatilaka, D.; Spackman, M. A. *CrystalExplorer*: a program for Hirshfeld surface analysis, visualization and quantitative analysis of molecular crystals. *J. Appl. Crystallogr.* **2021**, *54*, 1006–1011.

[24]. Etsè, K. S.; Dorosz, J.; McLain Christensen, K.; Thomas, J.-Y.; Botez Pop, I.; Goffin, E.; Colson, T.; Lestage, P.; Danober, L.; Pirotte, B.; Kastrup, J. S.; Francotte, P. Development of thiochroman dioxide analogues of benzothiadiazine dioxides as new positive allosteric modulators of α-amino-3-hydroxy-5-methyl-4-isoxazolepropionic acid (AMPA) receptors. *ACS Chem. Neurosci.* **2021**, *12*, 2679–2692.

[25]. DeLano, W. L. The PyMOL Molecular Graphics System, DeLano Scientific, 700, San Carlos, CA, 2002.

[26]. Qi, H. W.; Kulik, H. J. Evaluating unexpectedly short non-covalent distances in X-ray crystal structures of proteins with electronic structure analysis. *J. Chem. Inf. Model.* **2019**, *59*, 2199–2211.

[27]. Scheiner, S. Understanding noncovalent bonds and their controlling forces. *J. Chem. Phys.* **2020**, *153*, 140901.

[28]. Spackman, P. R.; Yu, L.-J.; Morton, C. J.; Parker, M. W.; Bond, C. S.; Spackman, M. A.; Jayatilaka, D.; Thomas, S. P. Bridging crystal engineering and drug discovery by utilizing intermolecular interactions and molecular shapes in crystals. *Angew. Chem. Int. Ed Engl.* **2019**, *58*, 16780–16784.

[29]. Mandal, S. K.; Saha, P.; Munshi, P.; Sukumar, N. Exploring potent ligand for proteins: insights from knowledge-based scoring functions and molecular interaction energies. *Struct. Chem.* **2017**, *28*, 1537–1552.

[30]. Hunter, C. A.; Singh, J.; Thornton, J. M. Π-π interactions: The geometry and energetics of phenylalanine-phenylalanine interactions in proteins. *J. Mol. Biol.* **1991**, *218*, 837–846.

[31]. Spackman, M. A.; McKinnon, J. J. Fingerprinting intermolecular interactions in molecular crystals. *CrystEngComm* **2002**, *4*, 378–392.

[32]. Spackman, M. A.; Jayatilaka, D. Hirshfeld surface analysis. *CrystEngComm* **2009**, *11*, 19–32.

[33]. Etsè, K. S.; Etsè, K. D.; Nyssen, P.; Mouithys-Mickalad, A. Assessment of anti-inflammatory-like, antioxidant activities and molecular docking of three alkynyl-substituted 3-ylidene-dihydrobenzo[d]isothiazole 1,1-dioxide derivatives. *Chem. Biol. Interact.* **2021**, *344*, 109513.

[34]. Sénam Etsè, K.; Zaragoza, G.; Boschini, F.; Mahmoud, A. New N-methylimidazolium hexachloroantimonate: Synthesis, crystal structure, Hirshfeld surface and catalytic activity of in cyclopropanation of stryrene. *Inorg. Chem. Commun.* **2020**, *122*, 108291.

[35]. Etsè, K. S.; Zaragoza, G. Insight into structural description of novel 1,4-Diacetyl-3,6-bis(phenylmethyl)-2,5-piperazinedione: synthesis, NMR, IR, Raman, X-ray, Hirshfeld surface, DFT and docking on breast cancer resistance protein. *J. Mol. Struct.* **2022**, *1248*, 131435.

[36]. Etsè, K. S.; Demonceau, A.; Zaragoza, G.; Serteyn, D.; Mouithys-Mickalad, A. Design, synthesis and biochemical evaluation of novel 2-amino-3-(7-methoxybenzo[d][1,3]dioxol-5-yl)propanoic acid using Horseradish peroxidase (HRP) activity, cellular ROS inhibition and molecular docking study. *J. Mol. Struct.* **2022**, *1250*, 131668.

[37]. Etsè, K. S.; Zaragoza, G.; Etsè, K. D. Easy preparation of novel 3,3-dimethyl-3,4-dihydro-2H-1,2,4-benzothiadiazine 1,1-dioxide: Molecular structure, Hirshfeld surface, NCI analyses and molecular docking on AMPA receptors. *J. Mol. Struct.* **2021**, *1238*, 130435.

[38]. Etse, K. S.; Lamela, L. C.; Zaragoza, G.; Pirotte, B. Synthesis, crystal structure, Hirshfeld surface and interaction energies analysis of 5-methyl-1,3-bis(3-nitrobenzyl)pyrimidine-2,4(1H,3H)-dione. *Eur. J. Chem.* **2020**, *11*, 91–99.

[39]. McKinnon, J. J.; Jayatilaka, D.; Spackman, M. A. Towards quantitative analysis of intermolecular interactions with Hirshfeld surfaces. *Chem. Commun. (Camb.)* **2007**, 3814–3816.

[40]. Tan, S. L.; Jotani, M. M.; Tiekink, E. R. T. Utilizing Hirshfeld surface calculations, non-covalent interaction (NCI) plots and the calculation of interaction energies in the analysis of molecular packing. *Acta Crystallogr. E Crystallogr. Commun.* **2019**, *75*, 308–318.

[41]. Ifeanyieze, K. J.; Ayiya, B. B.; Okpareke, O. C.; Groutso, T. V.; Asegbeloyin, J. N. Crystal structure, Hirshfeld surface and computational study of 1-(9,10-dioxo-9,10-dihydroanthracen-1-yl)-3-propanoylthiourea. *Acta Crystallogr. E Crystallogr. Commun.* **2022**, *78*, 439–444.

[42]. Ayiya, B. B.; Okpareke, O. C. N,N'-Di(pyridine-4-yl)-pyridine-3,5-dicarboxamide, a pincer-type tricationic compound; Synthesis, crystal structure, Hirshfeld surface analysis, and computational chemistry studies. *J. Chem. Crystallogr.* **2021**, https://doi.org/10.1007/s10870-021-00902-4.

[43]. Turner, M. J.; Thomas, S. P.; Shi, M. W.; Jayatilaka, D.; Spackman, M. A. Energy frameworks: insights into interaction anisotropy and the mechanical properties of molecular crystals. *Chem. Commun. (Camb.)* **2015**, *51*, 3735–3738.

[44]. Mackenzie, C. F.; Spackman, P. R.; Jayatilaka, D.; Spackman, M. A. *CrystalExplorer* model energies and energy frameworks: extension to metal coordination compounds, organic salts, solvates and open-shell systems. *IUCrJ* **2017**, *4*, 575–587.